equilibrium-derived triplet-state energies may be understood in terms of the spin statistical factor. Thus, in going from $SiNC(T_1)$ to $O_2(^1\Delta_g)$ only one-ninth of the intervening collision complexes are of overall singlet multiplicity, whereas for the reverse process there are only uniquely singlet complexes. This effect results in the equilibrium-derived T_1 energy value being depressed from the spectroscopic value by a factor of $RT \ln (^1/_9) = 1.3$ kcal/mol at 24 °C. This brings the two values in line.

Conclusion

This work confirms our earlier preliminary conclusion that energy transfer from the triplet state of SiNC to O_2 to produce singlet oxygen is a reversible reaction. A kinetic model for the reaction satisfactorily accounts for the results of laser flash photolysis experiments and makes it possible to evaluate the rate and equilibrium constants. This model is supported by the fact that the kinetic parameters obtained are independent of whether the equilibrium is approached by generating $SiNC(T_1)$ first (in the presence of $O_2(^3\Sigma_g^-)$) or by generating $O_2(^1\Delta_g)$ first (in the presence of $SiNC(S_0)$). Although energy transfer from $SiNC(T_1)$ to $O_2(^3\Sigma_g^-)$ is endergonic, the efficiency of conversion of the triplets into singlet oxygen is nearly 100% because the SiNC triplet is intrinsically long-lived and the equilibrium state is drained mainly via the decay of $O_2(^1\Delta_g)$.

Acknowledgment. The laser flash photolysis and data analyses were carried out at the Center for Fast Kinetics Research at the University of Texas at Austin. The CFKR is supported jointly by NIH Grant RR 00886 from the Biotechnology Branch of the Division of Research Resources and by the University of Texas at Austin. Support for this project came from NIH Grant GM 24235. We thank Dr. A. A. Gorman for enlightening discussions.

Registry No. O_2, 7782-44-7; SiNC, 92396-88-8.

Photoelectrochemistry of Strained-Layer and Lattice-Matched Superlattice Electrodes: Effects Due to Buffer Layers

A. J. Nozik,* B. R. Thacker, J. A. Turner, and M. W. Peterson

Contribution from the Solar Energy Research Institute, Golden, Colorado 80401.
Received April 25, 1988

Abstract: Strained-layer and lattice-matched superlattice electrodes have been studied and compared as photoelectrodes in photoelectrochemical cells, and the effects of the presence of buffer layers in the strained-layer systems have been established. Photocurrent spectroscopy and photomodulated reflectance spectroscopy of superlattice electrodes, etched superlattice electrodes, and buffer layer structures reveal that highly strained superlattices (1.8% mismatch) have poorly defined quantization effects in their quantum wells; strained-layer superlattices with less mismatch (0.9%) have better defined quantization, but this is not reflected in their photocurrent spectra. On the other hand, lattice-matched superlattice electrodes exhibit extremely well-defined quantization effects that are clearly exhibited in multiple photocurrent peaks that match theoretical predictions; photomodulated reflectance spectra exhibit 17 transitions that represent all the possible allowed transitions in the quantum wells, including all light and heavy hole transitions, as well as unconfined transitions above the well barriers. The present work indicates that previous results reported for the photoelectrochemistry of highly strained superlattices probably reflected a photoresponse that was influenced more by the buffer layers than by the superlattice layers. The occurrence of hot electron transfer from photoexcited superlattice electrodes remains to be demonstrated unequivocally.

The photocurrent action spectra of superlattice electrodes in photoelectrocheical cells have been reported[1-3] to exhibit interesting features that have been attributed to the presence of discrete energy level structure in the quantum wells of the superlattice. Results with both lattice-matched superlattices (LMS), consisting of GaAs quantum wells and $Al_{0.38}Ga_{0.62}As$ barriers,[1] and strained-layer superlattices (SLS), consisting of GaAs wells and $GaAs_{0.5}P_{0.5}$ barriers,[2,3] have been described.

Because of the lattice mismatch between the GaAs and $GaAs_{0.5}P_{0.5}$ layers, strained-layer superlattices require a series of buffer layers between the single-crystal substrate and the superlattice that are graded in composition in order to provide a composition for the last buffer layer that is equal to the average composition of the superlattice layers; this is necessary to minimize misfit dislocations and produce good morphology in the superlattice.[4] Lattice-matched superlattices do not require such a series of buffer layers; the superlattice is simply grown on top of a single GaAs epilayer deposited on a GaAs single-crystal substrate.

In our previous study of SLS electrodes,[2,3] they consisted of a single-crystal p^+–GaAs substrate, a nondeliberately doped GaAs epilayer, five nondeliberately doped buffer layers, and a 20-period superlattice with 250-Å GaAs wells and either 250- and 40-Å $GaAs_{0.5}P_{0.5}$ barriers. We assumed that the observed photocurrent from these electrodes was generated only in the superlattice layers, and we completely neglected any contributions from the underlying $GaAs_{1-x}P_x$ buffer layers or from a possible p–n junction between the p^+-GaAs substrate and the undoped p-GaAs epilayer. This assumption would be valid for cathodic photocurrent in our particular sample configuration if the buffer layers are p-type, since under these conditions electrons must flow against a series of potential barriers created by the heterojunctions between the buffer layers. Although Mott-Schottky data for our SLS electrodes indicated p-type character over the potential regions where the photocurrent is cathodic, we have found recent experimental results that indicate the buffer layers behave n-type and contribute significant photocurrent at wavelengths above 775 nm. Furthermore, a fortuitous complication is that the band gaps of the five $GaAs_{1-x}P_x$ buffer layers in our samples overlap some of the theoretical energy transitions for the GaAs quantum wells in our superlattices. These quantum wells comprise a total thickness of 0.5 μ and absorb between 40 and 60% of the incident light between 850 and 700 nm, respetively; the rest of the light passes

(1) Nozik, A. J.; Thacker, B. R.; Turner, J. A.; Klem, J.; Morkoc, H. *Appl. Phys. Lett.* **1987**, *50*, 34.
(2) Nozik, A. J.; Thacker, B. R.; Turner, J. A.; Olson, J. M. *J. Am. Chem. Soc.* **1985**, *107*, 7805.
(3) Nozik, A. J.; Thacker, B. R.; Olson, J. M. *Nature (London)* **1985**, *316*, 6023, **1987**, *326*, 450.
(4) Matthews, J. W.; Blakeslee, A. E.; Mader, S. *Thin Solid Films* **1976**, *33*, 253. Osbourn, G. C. *J. Vac. Sci. Techol.* **1982**, *21*, 469.

0002-7863/88/1510-7630$01.50/0

into the buffer layer regions. Therefore, our prior observations and conclusions[2,3] on SLS electrodes are clouded by unrecognized photocurrent contributions from the buffer layers.

In this paper we examine the effects of buffer layers in SLS electrodes in detail and attempt to separate them from effects due only to the superlattice region. We examine SLS samples where the superlattice has been progressively etched away, as well as electrodes that consist only of buffer layers; we also study deliberately p-doped epilayers and buffer layers.

Since strained-layer superlattices can have large differences in the lattice constant between the wells and barriers (1.8% lattice mismatch for $GaAs/GaAs_{0.5}P_{0.5}$), they can exhibit poor morphology in the form of nonparallel, discontinuous, and/or wavy layers. To check whether poor morphology in our SLS electrodes affects the formation of well-defined quantization in the quantum wells, we examined our samples using photomodulated reflectance (PR) spectroscopy. This technique provides very powerful information on the character and quality of quantization effects in superlattices.[5] We also studied the SLS electrodes in the form of solid-state Schottky junctions to determine the influence of liquid versus solid junctions on the spectral characteristics of the photocurrent response.

Our studies have also been extended to LMS electrodes that do not contain a series of graded buffer layers. In these samples we examine the contributions due to the single GaAs epilayer through deliberate p-doping and etching studies, and compare PR results with the photocurrent spectroscopy of both liquid- and solid-state junctions.

Finally, we reexamine the conclusions of our previous papers[1-3] concerning experimental evidence for hot electron transfer from the high-lying quantum states of the superlattice electrodes into the liquid electrolyte.

Experimental Section

The SLS electrodes were made by metalloorganic chemical vapor deposition (MOCVD). The superlattice samples consisted of 20 periods of alternating 250-Å layers of GaAs and $GaAs_{1-x}P_x$, with a total superlattice thickness of 1 μ. GaAs has a band gap (E_g) of 1.42 eV and forms a quantum well structure when sandwiched between $GaAs_{1-x}P_x$ barriers. A high-barrier SLS contained $GaAs_{0.5}P_{0.5}$ barriers having a band gap of 2.0 eV. The electron and hole barrier heights are divided almost equally at about 0.3 eV. A lower barrier structure was grown with $GaAs_{0.75}P_{0.25}$ barriers (E_g = 1.72 eV); this sample had about half the lattice mismatch (0.9%) and about half the barrier heights (150 meV) of the sample containing $GaAs_{0.5}P_{0.5}$.

The buffer layer structure for the large barrier SLS consisted of 10 μm of $GaAs_{1-x}P_x$ graded from x = 0.05 to 0.25 in five equal 2-μm steps; it was grown between a 0.5-μm undoped GaAs epilayer deposited on the p^+-GaAs single-crystal substrate and the $GaAs_{0.5}P_{0.5}$ 20-period SLS. p^+ buffer layers or SLS layers were also grown by incorporating 1×10^{18} cm^{-3} of Zn. A sample with nondeliberately doped buffer layers was made without the SLS structure in order to study the photocurrent behavior of this structure alone. The background electron density for these nondeliberately doped buffer layers was estimated at 10^{15} to 10^{16} cm^{-3} based on Mott–Schottky data. For the low-barrier sample, two buffer layers of $GaAs_{1-x}P_x$ with x = 0.06 and 0.12 were deposited before the superlattice.

The compositions and thicknesses of the layers were established by calibrating the flow rates and temperatures of the gases in the MOCVD against resultant III–V layer compositions determined by ion beam microprobe analysis.

The lattice-matched superlattice (LMS) electrodes were made by molecular beam epitaxy (MBE) and consisted of alternating layers of GaAs wells and $Al_{0.38}Ga_{0.62}As$ barriers deposited upon a p^+-GaAs substrate coated with a single undoped 0.4-μm GaAs epilayer. The GaAs wells were 250 Å thick, and samples were grown with both thick and thin barriers that were 250 and 40 Å, respectively. LMS samples with a single p^+-GaAs epilayer were also grown by doping the 0.4-μm epilayer with zinc.

Procedures for mounting the electrodes and measuring photocurrents in aqueous solutions were described previously.[1-3] Nonaqueous experiments were performed in a Vacuum Atmospheres drybox using Burdick and Jackson spectral grade acetonitrile distilled in calcium hydride, and then passed over activated alumina in the box. A silver wire reference electrode was used for all nonaqueous experiments and its potential monitored by comparison with the formal redox potential of the ferricinium/ferrocene couple, whose $E°$ was 190 mV positive of the silver reference. Tetraethylammonium fluoroborate ($TEABF_4$) from Southwest Analytical Laboratories was dried under vacuum and used as the supporting electrolyte. Ferrocene (Aldrich) was purified by sublimation. Cobalticenium hexafluorophosphate (Strem) was used without further purification. Purified ferricinium hexafluorophosphate and cobaltocene were generously provided by C. Curtis of SERI. In aqueous electrolyte, all potentials are reported versus SCE.

To remove the superlattice layers, SLS and LMS electrodes were etched in fresh 6:1:1 $H_2SO_4/H_2O_2/H_2O$ at room temperature with gentle stirring and quenched immediately after the etch in doubly deionized water. The etch rate for the $GaAs/GaAs_{0.5}P_{0.5}$ SLS electrodes (250-Å well, 250-Å barrier) was determined by mounting them in Apieson black wax, etching for different times, removing the wax, and then measuring the etch step with a Sloan M-200 angstrometer. The etch rate appeared to decrease with greater etching times but averaged about 1.2 μ/min.

Solid-state junctions were formed by evaporating thin (150-Å) gold layers on top of the superlattice electrodes to form Schottky barriers. They were mounted in a liquid nitrogen dewar and the photocurrent spectra were recorded as a function of temperature.

Photomodulated reflectance (PR) spectroscopy was accomplished by chopping a laser pump beam having a photon energy above the band gap of the well (488-nm Ar ion-laser, 1.4 mW) to modulate the space charge layer, and then measuring the reflectance of a second superimposed light beam as a function of wavelength using phase-sensitive lock-in techniques. The probe beam was obtained by passing the output of a 250-W tungsten lamp through a monochromator; the PR experiments were conducted with the samples sitting freely in air. The resulting PR spectra are extremely sensitive to the optical constants and show derivative-like spectra.[5]

The PR spectra were fitted to Aspnes' generalized derivative form:[5]

$$\Delta R/R = \mathrm{Re}\{\sum_j [C_j e^{i\theta_j}(E - E_{g,j} + i\Gamma_j)^{-n_j}]\} \quad (1)$$

where subscript j refers to the jth transition, C is the amplitude, E_g is the transition energy, Γ is the broadening parameter, θ is the phase, and n denotes the type of critical point for the transition and the order of its derivative. The value of n depends upon whether the transitions involve localized (e.g., excitonic) or delocalized states (e.g., minibands). Because of the large number of transitions in our samples and their close spacing, the PR spectra could be fitted equally well with the various possible values of n; i.e., n could not be uniquely determined. The transition energies are of most interest in this work and their values are indicated by arrows in the figures showing fitted PR spectra (Figures 6 and 9) and in Tables II–IV.

The theoretical energy levels in the electron and hole quantum wells and the corresponding optical transitions were calculated using the two-band envelope function model of Bastard.[6] This calculation predicts the heavy and light hole transition energies; it also determines the broadening (i.e., dispersion) of the quantum states into minibands due to the coupling between wells and charge delocalization when the barriers are sufficiently thin ($<\sim$50 Å). The latter effect results in a splitting of the optical transitions seen in PR spectra that arise from critical point transitions occurring from both the center of the miniband Brillouin zone (denoted Γ transition) and from the edge of the miniband Brillouin zone (denoted Π transition).[5] The model also predicts the existence of quantized states for electrons and holes *above* their respective barriers. These are labeled as unconfined states; states in the well, even when delocalized because of miniband formation, are referred to as confined states.

Results

Strained Layer Superlattices. Figure 1 shows the photocurrent spectra for an electrode that consists only of nondeliberately doped buffer layers at −1 V (Figure 1a) and 0 V (Figure 1b) in 1 M H_2SO_4. The arrows identify each of the five buffer layer band-gap energies as calculated from their estimated compositions (see Table I). The cathodic photocurrent spectrum at −1 V has an onset at the band-gap transition of GaAs ($\sim$875 nm), but then the

(5) Aspnes, D. E. In *Handbook on Semiconductors*; Moss, T. S., Ed.; North Holland: New York, 1980, Vol. 2. Glembocki, O. J.; Shanabrook, B. V.; Bottka, N.; Beard, W. T.; Comas, J. *Appl. Phys. Lett.* **1985**, *45*, 970. See also: *Proceedings of the Society of Photo-Optical Instrumentation Engineers*; SPIE: Bellingham, 1985; Vol. 524, p 86. Pollak, F. H. *Ibid.* 1981; Vol. 276, p 142. Parayanthal, P.; Shen, H.; Pollak, F. H.; Glenbocki, O. J.; Shanabrook, B. V.; Beard, W. T. *Appl. Phys. Lett.* **1986**, *48*, 1261.

(6) Bastard, G. *Phys. Rev. B* **1982**, *25*, 7584; **1981**, *24*, 5693. Bastard, G.; Brum, J. A. *IEEE J. Quantum Electron* **1986**, *QE-22*, 1625.

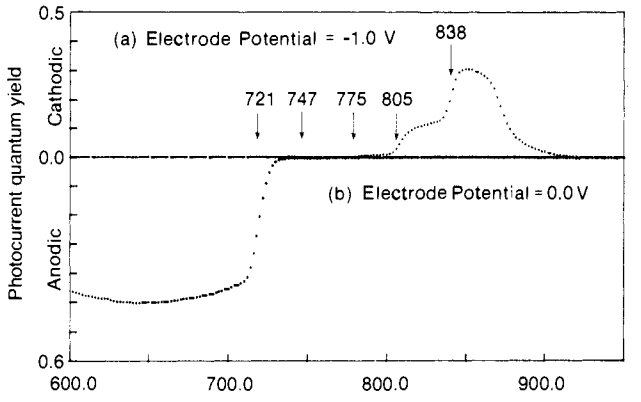

Figure 1. Photocurrent spectra of electrode consisting only of five buffer layers of $GaAs_{1-x}P_x$ deposited on a GaAs epilayer. The buffer layers are 2 μm thick and graded in five equal steps from $x = 0.05$ to 0.25. The band gaps of these five buffer layers are indicated by arrows in the figure. The electrolyte is 1 M H_2SO_4; the electrode potentials are versus SCE.

Table I. Buffer Layer Band Gaps and Quantum Well Transition Energies in SLS with $GaAs_{0.5}P_{0.5}$ (2.0 eV) Barriers

$GaAs_{1-x}P_x$ buffer layers			
	E_g		theoretical transitions in
x	eV	nm	quantum wells ($\Delta n = 0$), eV
0.05	1.48	838	1.429
0.10	1.54	805	1.456
0.15	1.60	775	1.500
0.20	1.66	747	1.562
0.25	1.72	721	1.639
			1.728

photocurrent drops in three steps at 842, 815, and 780 nm. These three steps are associated with the three lowest band gaps of the first three buffer layers. At 0 V, the anodic photocurrent has an onset at 730 nm, rises sharply, and then plateaus at 710 nm; this photocurrent is associated with excitation of the last (outermost) buffer layer. At potentials between 0 and −1 V the photocurrent spectra showed both anodic and cathodic regions.

Mott-Schottky, Hall effect, and i-v data for single $GaAs_{1-x}P_x$ epilayers indicate that the material is n-type as grown in the MOCVD reactor without intentional doping; the calculated background doping levels are 10^{15} to 10^{16} cm^{-3}.

Several SLS electrodes were etched to remove the superlattice layers, and changes in the photocurrent spectra were observed in order to distinguish directly photocurrents originating in the superlattice. In Figure 2 we show results for a 2.0-eV barrier SLS sample at −2 V (cathodic photocurrent, Figure 2A) and at +0.3 V (anodic photocurrent, Figure 2B) versus silver wire; results are presented for an unetched sample and after 90 s in (6:1:1) H_2SO_4. The solution was 1 mM ferricinium/1 mM ferrocene in acetonitrile. The quantum yield increases with etching throughout the cathodic spectra, showing more distinctive structure at lower energy. For the anodic spectrum, a new step appears in the spectra of the etched sample at +0.3 V, with an onset at 750 nm; this mirrors a cathodic step that is present in both etched and unetched spectra. At shorter wavelengths, the etched spectra are flat below 700 nm, displaying none of the decreasing anodic photocurrent present in most of the unetched samples. The only region where etching decreased the photocurrent is in the anodic photocurrent at longer wavelengths between 750 and 825 nm.

Etch studies were also performed on the superlattices with 1.7-eV barriers (250-Å GaAs/250-Å $GaAs_{0.75}P_{0.25}$) that contain only two buffer layers instead of five. Figure 3 shows cathodic and anodic spectra at −3.0 and +0.5 V, respectively, after the etch times indicated in the figure. The experiments were done with 0.1 M ferrocene in acetonitrile. The results (Figure 3B) show an initial decrease in the anodic photocurrent between 770 to 860 nm after the first 80 s of etching, creating a large photocurrent step at 770 nm. After further etching (Figure 3D) the anodic photocurrent above 770 nm begins to increase. After 150 s, the

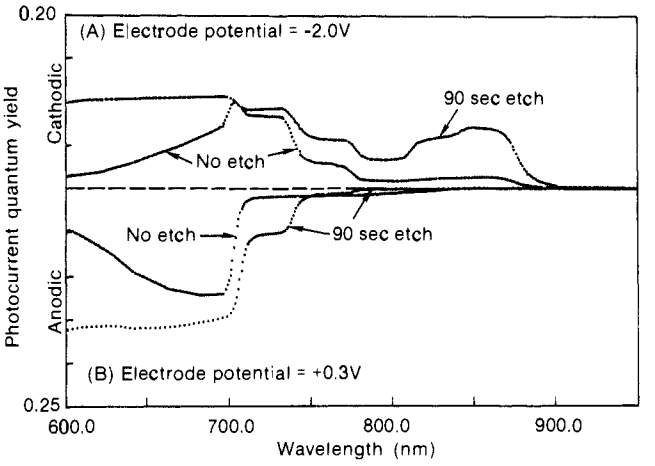

Figure 2. Effects of etching on photocurrent spectra of SLS electrodes with $GaAs_{0.5}P_{0.5}$ barriers (2.0 eV): (A) cathodic photocurrent, (B) anodic photocurrent. The electrolyte is 1 mM ferricinium/ferrocene in acetonitrile; the reference electrode is Ag wire.

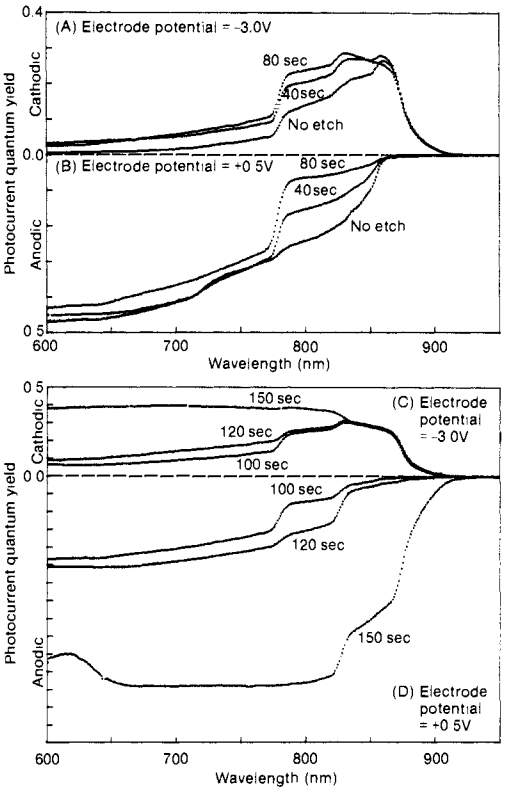

Figure 3. Effects of etching on photocurrent spectra of SLS electrodes with $GaAs_{0.75}P_{0.25}$ barriers (1.72 eV): (A and C) the cathodic photocurrents after various indicated etching times; (B and D) the anodic photocurrents after various indicated etching times. The electrolyte is 0.1 M ferrocene in acetonitrile; the reference is Ag wire.

anodic photocurrent above 770 nm has increased markedly with a strong onset at about 900 nm.

The cathodic experiments followed the anodic experiments after each etch time. As seen in Figure 3, A and C, an increase occurs in the cathodic photocurrents at wavelengths <860 nm that continues to grow with longer etching times; after 150 s the photocurrent has reached a constant value for $\lambda < 825$ nm. A small decrease in the cathodic photocurrent occurs above 850 nm during the first 80 s of etching.

A 250-Å GaAs/250-Å $GaAs_{0.5}P_{0.5}$ superlattice was grown with the five buffer layers doped p-type. At potentials of −0.4 V the cathodic photocurrent spectra has an onset at 860 nm and a gradual step at 680 nm (see Figure 4). After etching this electrode for 2 min, the cathodic photocurrent between 860 and 750 nm is eliminated. Anodic photocurrents appear only at potentials

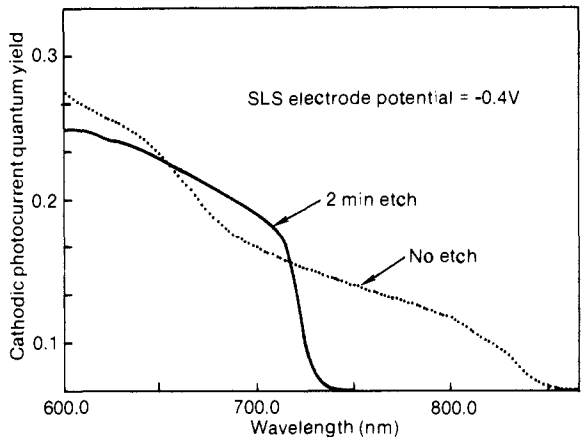

Figure 4. Effects of etching on the photocurrent spectra of 2.0-eV barrier SLS electrodes with p-doped buffer layers. The electrolyte is 1 M H_2SO_4 and the reference electrode is SCE.

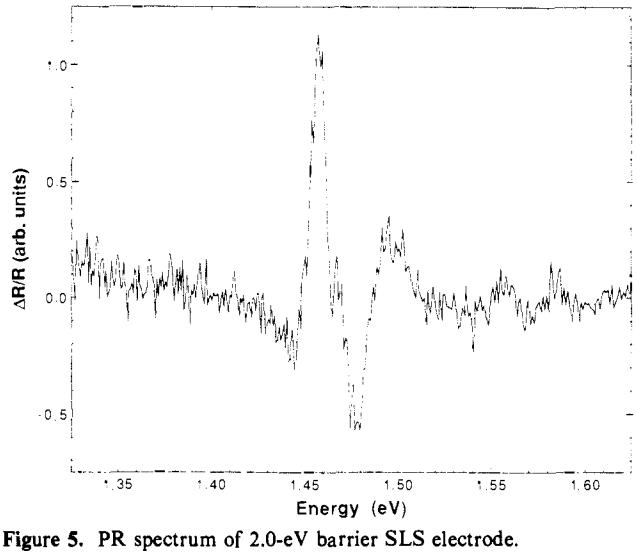

Figure 5. PR spectrum of 2.0-eV barrier SLS electrode.

Table II. Comparison of Optical Transitions from PR Spectra of SLS with $GaAs_{0.75}P_{0.25}$ (1.72 eV) Barriers with Buffer Layer and Theoretical Quantum Well Transitions

PR transition energies, eV	$GaAs_{1-x}P_x$ buffer layer		theoretical well transitions ($\Delta n = 0$), eV
	x	E_g, eV	
1.442	0.06	1.494	1.428
1.460	0.12	1.561	1.453
1.476			1.493
1.490			1.547
1.509			1.605
1.541			
1.630			

where high anodic dark currents occur, accompanied by dissolution of the electrode surface.

PR spectra are shown in Figures 5 and 6 for the two SLS samples with the 2.0- and 1.7-eV barrier heights, respectively. The latter spectra could be fitted very well to seven transitions using the generic Aspnes expression[5] in eq 1; the peak positions are listed in Table II. The PR spectra from the 2.0-eV barrier sample were very noisy and poorly defined; a meaningful fit to these data could not be achieved. This is attributed in part to poor morphology that generates a high degree of scattered light from the surface and a weak signal-to-noise ratio (see Discussion).

Photocurrent spectra for a gold Schottky barrier contact to the 1.7-eV barrier sample showed the same spectrum as for the liquid junction at both room temperature and 77 K, except that the latter spectrum was blue-shifted due to the lower temperature. The spectrum for the 2.0-eV barrier SLS sample was also the same

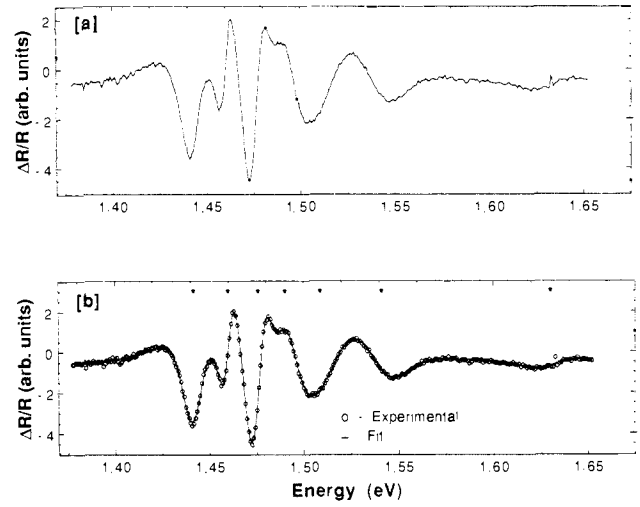

Figure 6. PR spectrum of 1.72-eV barrier SLS electrode showing theoretical fit to seven optical transitions.

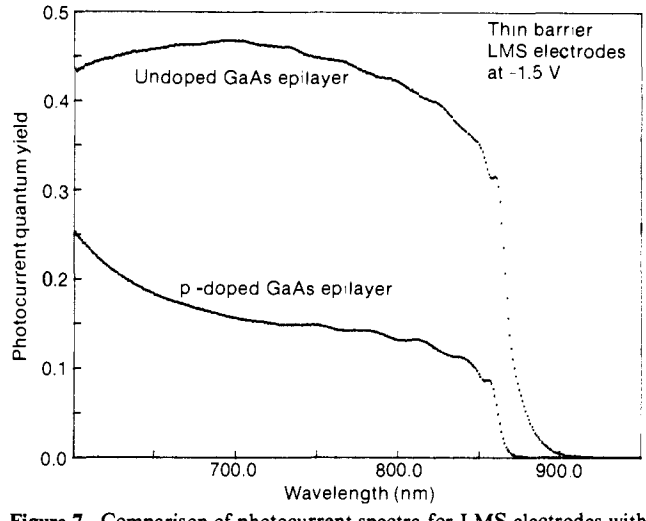

Figure 7. Comparison of photocurrent spectra for LMS electrodes with thin (40 Å) barriers containing undoped and p-doped GaAs epilayers.

for liquid and solid contacts; it was measured only at room temperature in both cases.

Lattice-Matched Superlattice. Photocurrent spectra for lattice-matched samples were obtained with both undoped and p-doped GaAs epilayers, and on samples with 40- and 250-Å barriers. All photocurrents observed with these electrodes were cathodic; no anodic photocurrents were seen even in the region where anodic dissolution begins. The results for the LMS electrodes with the undoped GaAs epilayer were published previously.[1] A comparison of photocurrent spectra for 40-Å barrier samples with p-doped and undoped GaAs epilayers is shown in Figure 7. Both spectra were obtained at −1.5 V versus a silver wire reference electrode, in 2 mM cobalticenium in acetonitrile. The electrode with the undoped GaAs epilayer has a photocurrent onset at 900 nm, rising sharply to a peak at 860 nm, followed by a gradual rise containing a series of very small peaks at higher energy; these peaks are not easily seen in Figure 7 and require a more sensitive scale for observation (see Figure 1 in ref 1). The sample with the p-doped GaAs epilayer has similar spectral features, but the onset does not occur until 875 nm and the plateau photocurrent has only about one-third the quantum yield of the undoped buffer layer sample. Both spectra were obtained at a cathodic bias where the current voltage curves were in the saturated plateau region.

At less negative potentials, the photocurrent spectra for the lattice-matched samples are somewhat better resolved. Figure 8, A and B, shows the spectra for thick barrier samples with the p-doped epilayer at −0.5 and −1.0 V, respectively; the spectrum in Figure 8C is for the thin-barrier LMS with a p-doped epilayer at −1.0 V.

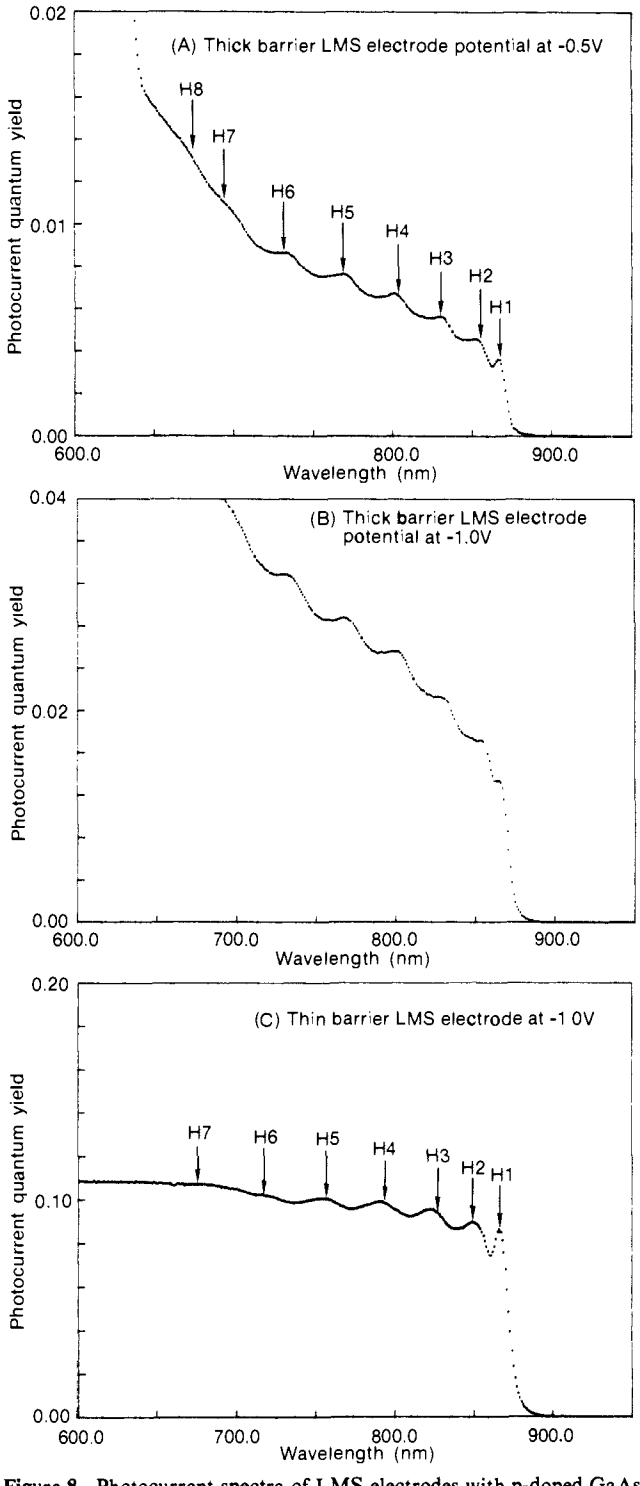

Figure 8. Photocurrent spectra of LMS electrodes with p-doped GaAs epilayers: (A) thick-barrier (250 Å) sample at −0.5 V; (B) thick-barrier sample at −1.0 V; (C) thin-barrier (40 Å) sample at −1.0 V. For (A), arrows show theoretical allowed ($\Delta n = 0$) transitions from heavy-hole states to electron states in the quantum wells with a well width of 265 Å. For (C), arrows show theoretical allowed ($\Delta n = 0$) transitions from heavy-hole states to electron states with a well width of 250 Å.

For LMS electrodes with p-doped epilayers, the quantum yields of the thin-barrier electrodes are much higher than those of the thick-barrier samples, as they were with electrodes having undoped epilayers. As seen in Figure 8 both thick- and thin-barrier samples exhibit well-resolved peaks in their photocurrent spectra. The theoretically calculated allowed ($\Delta n = 0$) transitions from heavy hole states to electron states in the wells are indicated in the figures as arrows; the theoretical values are based on GaAs wells of 265 and 250 Å for the thick- and thin-barrier LMS electrodes, respectively; Table III summarizes the results.

Table III. Comparison of Calculated Transition Energies with Observed Photocurrent Peaks for LMS Electrodes

theoretical transition energies, eV, at barrier thickness		observed peaks in photocurrent spectra, eV, barrier thickness	
250 Å[a]	40 Å[b]	250 Å	40 Å
1.428	1.429	1.43	1.43
1.451	1.455	1.45	1.46
1.491	1.498	1.49	1.51
1.545	1.559	1.55	1.57
1.615	1.631, 1.642[d]	1.61	1.64
1.698	1.740, 1.720[d]	1.69	1.73
1.790	1.820, 1.855[c,d]	1.77	1.78
1.837[c]		1.85	

[a] Based on 265-Å well width. [b] Based on 250-Å well width. [c] Unconfined transitions. [d] Doublets due to miniband dispersion.

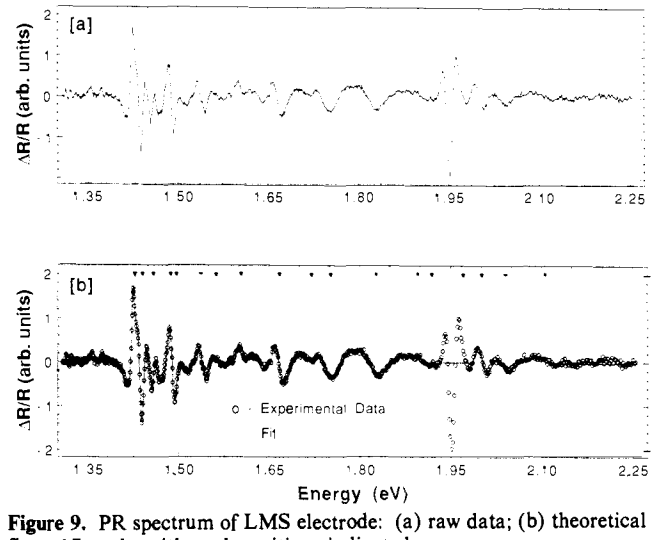

Figure 9. PR spectrum of LMS electrode: (a) raw data; (b) theoretical fit to 17 peaks with peak positions indicated.

The photocurrents of LMS electrodes with p-doped epilayers were measured in both cobalticenium and ferricenium; however, the electrodes were not stable in ferricenium, and reproducible spectra could not be obtained. Instead a comparison was made between cobalticenium and decamethylferricenium, which have redox potentials that differ by 0.8 V (−1.13 and −0.34 V, respectively). Reproducible spectra were obtained with decamethylferricinium that differed insignificantly from the cobaltocinium results.

LMS electrodes of both barrier thicknesses were etched at 1-min intervals to check the effect of the underlying epitaxial buffer layer and substrate. The photocurrent structure in both samples gradually diminished with etch time and after 3 min etching had disappeared.

The PR spectrum of the LMS electrode with the p^+-doped epilayer and 250-Å barriers is shown in Figure 9. The spectrum exhibits very rich structure which fits very well to 17 peaks over the energy range of 1.42 to 2.11 eV. These peaks correspond extremely well to *all* the theoretically calculated allowed ($\Delta n = 0$) transitions confined in the quantum well, including all heavy and light hole transitions and transitions involving unconfined states *above* the barriers for electrons and/or holes at photon energies >1.75 eV. The observed and calculated transition energies are listed in Table IV; the calculated transitions are based on a well width of 285 Å. The notation we use for a given transition is H (or L) *n*, *m*, where H refers to heavy holes and L refers to light holes in the GaAs valence band, and *n* and *m* refer to the quantum states of the holes and electrons, respectively; the selection rule for allowed transitions is $\Delta n = 0$, and thus *n* for the hole states = *m* for the electron states. A U before the H or L indicates that the transition involves unconfined states above the hole barrier; a U before the *m* indicates the transition involves unconfined states

Table IV. Observed Optical Transitions in Thick-Barrier LMS Electrodes from Fit of PR Spectra Compared with Theoretically Calculated Allowed Transitions[a]

exptl transition energies from PR spectra, eV	calcd transition energy, eV	type
1.428	1.427	H1,1
1.429	1.430	L1,1
1.441	1.448	H2,2
1.459	1.460	L2,2
1.487	1.483	H3,3
1.497	1.509	L3,3
1.537	1.532	H4,4
1.563	1.580	L4,4
1.604	1.594	H5,5
1.668	1.669	L5,5
	1.668	H6,6
1.720	1.752	H7,7
1.752	1.773	L6,6
1.827	1.819	(Γ)H8,U8
	1.816	(Π)H8,U8
	1.827	(Γ)H9,U9
	1.858	(Π)H9,U9
1.897–1.920	1.898	(Π)H10,U10
	1.881	(Π)H10,U10
	1.889	L7,7
	1.932	(Γ)H11,U11
	1.949	(Π)H11,U11
b	1.983	(Γ)HL8,U8
	1.978	(Π)UL8,U8
2.001	1.992	(Γ)UL9,U9
	2.011	(Π)UL9,U9
	1.991	(Π)H12,U12
	2.013	(Γ)H12,U12
2.040	2.045	(Γ)UL10,U10
	2.018	(Π)UL10,U10
	2.064	(Γ)UL11,U11
	2.050	(Γ)H13,U13
	2.080	(Π)H13,U13
2.106	2.095	(Π)UL11,U11
	2.116	(Π)UL12,U12
	2.148	(Γ)H14,U14
	2.115	(Π)H14,U14

[a] Parameters for calculation: m_e = 0.0665, m_{hh}(well) = 0.34, m_{lh}(well) = 0.094, m_{hh}(barrier) = 0.50, m_{lh}(barrier) = 0.0982, E_g(well) = 1.42 eV, E_g(barrier) = 1.97 eV, electron barrier = 0.315 eV, hole barrier = 0.238 eV. [b] Well transition obscured by barrier transition.

above the electron barrier. A Γ or Π indicates the transition involves miniband dispersion, resulting in a doublet splting designated as Γ-type or Π-type.

Discussion

The band diagram for our SLS electrodes consisting of a p^+-GaAs substrate, a GaAs epilayer, and five $GaAs_{1-x}P_x$ buffer layers is shown in Figure 10. In Figure 10a, the band diagram is shown for n-type buffer layers, and in Figure 10b it is shown for p-type buffer layers. In the former case, the p^+-GaAs substrate and n-GaAs epilayer form a p–n junction, and the buffer layers form a series of five heterojunctions with the valence band edges producing a series of five potential barriers for holes that increase stepwise in the direction of the outer electrode surface; the conduction bands are aligned across the buffer layers with spiked discontinuities at the layer interfaces. For the p-doped buffer layer case, the valence bands are aligned with spiked discontinuities at the layer interfaces, and the conduction bands form a series of five potential barriers that increase stepwise in the direction toward the electrode surface; also, no p–n junction exists at the GaAs substrate–epilayer interface.

For both cases, the superlattice formed on top of the buffer layers is assumed to form a series of square wells and barriers, as usually assumed. The calculated energy levels for the quantum wells of the SLS using the Bastard model[6] are presented in Table I. For the case of the n-type buffer layer SLS, light with photon energy between the GaAs band gap (1.42 eV or 873.1 nm) and the band gap of the first buffer layer (1.494 eV or 830.0 nm) can be absorbed both in the GaAs wells in the superlattice structure

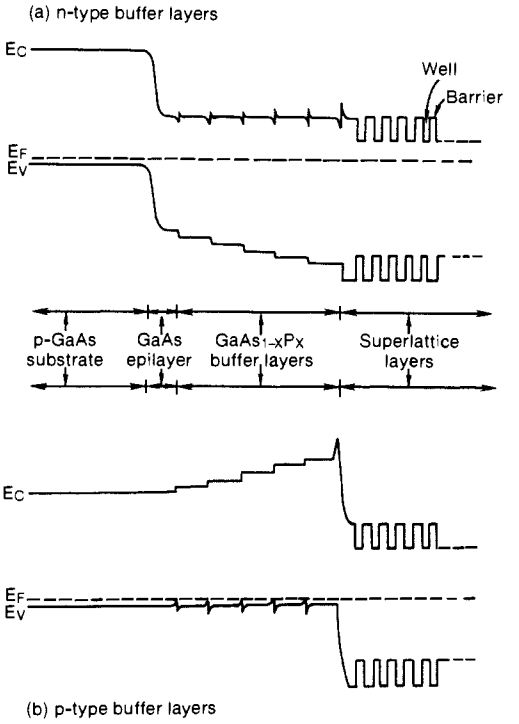

Figure 10. Energy band diagrams for SLS electrodes on a p-doped substrate with (a) n-doped epilayers and buffer layers, and (b) p-doped epilayers and buffer layers.

and at the GaAs p–n junction adjacent to the substrate. The relative distribution of this possible absorption will depend upon the total thickness of all the wells and that of the GaAs epilayer. For our SLS electrodes containing 20 superlattice periods with 250-Å GaAs wells, we estimate that, between 870 and 830 nm, the superlattice will absorb about 40% of the incident light, with the rest of the light passing through the buffer layers and being absorbed near the p–n junction. Under cathodic bias of the SLS electrode, electron-hole pairs created near the p–n junction will separate such that holes move to the substrate ohmic contact and electrons move toward the superlattice layers. Since the electrons are majority carriers in the buffer layer region, they can traverse it relatively easily, inhibited only by the spiked conduction band discontinuities at the layer interfaces. Thus, under negative bias a cathodic photocurrent can flow to the superlattice region by light absorption near the p–n junction that is 10–12 μm deep in the electrode structure.

Light with energy greater than the band gap of the first buffer layer (1.494 eV or 830.0 nm) can be absorbed both in the superlattice wells and in the various buffer layers, depending upon the wavelength. The cathodic photocurrent possible from light absorption in each buffer layer is expected to decrease with increasing band gap since the photogenerated minority holes must diffuse to the p–n junction at increasing distances with increasing band gap (see Figure 10a); the minority carrier diffusion length is typically 2–3 μm and the buffer layers are each 2 μm thick. Since the SLS electrodes have five buffer layers with band gaps close to the energy of some of the first five allowed transitions in the quantum well (Table I), the photocurrents arising from light absorption in n-type buffer layers will overlap and interfere with the transitions in the quantum well.

Under anodic bias, only holes photogenerated in the last buffer layer (1.72 eV) can make it to the liquid interface. Holes created in the lower band-gap buffer layers cannot reach the surface because they are blocked by a series of potential barriers. Hence, anodic photocurrent spectra will be free of interference effects from n-type buffer layers at photon energies below the band gap of the last buffer layer.

For the case of p-type buffer layers, the inverse of the above situation occurs. That is, under cathodic bias only electrons photogenerated in the last buffer layer with photon energies >1.72

eV can reach the liquid interface, while under anodic bias holes photogenerated in any of the buffer layers can reach the surface and contribute to the anodic photocurrent.

Since the buffer layers in our nondeliberately doped samples have been shown to be n-type because of unintentional doping during growth, they would be expected to behave as described above for n-type buffer layers (Figure 10a). The results in Figures 1–3 are consistent with this expectation.

Figure 1 shows the photocurrent spectrum of the buffer layers only. The cathodic photocurrent onset at 900 nm is associated with excitation of the p–n junction at the substrate–epilayer interface; the stepwise decrease in the cathodic photocurrent with increasing photon energy above 1.46 eV is associated with absorption in the buffer layers that increases stepwise as the photon energy successively reaches the band gap value of each buffer layer. Under anodic bias, no anodic photocurrent is observed until the photon energy reaches the value of the last buffer layer at 1.72 eV.

The etching experiments shown in Figures 2 and 3 directly check the contributions of the n-type buffer layers in SLS electrodes. For the small barrier SLS (Figure 3) under anodic bias, the initial etching (up to 80 s) decreases the anodic photocurrent between 860 and 770 nm. The photocurrent in this region is attributed to absorption in the superlattice and it decreases as the superlattice is removed by the etch. After 80 s the anodic photocurrent begins to increase between 770 and 900 nm; after 150 s there is a large increase in the anodic photocurrent with a steep onset at about 900 nm. The increase in the anodic photocurrent after 80 s is explained by progressive etching of the larger band gap buffer layers which forces the n-type semiconductor–liquid junction at the surface to be formed with progressively decreasing band gaps, thus creating an increased photoresponse at longer wavelengths. Under cathodic bias, the etching decreases the cathodic photocurrent only very slightly above 850 nm but increases the cathodic photocurrent markedly below 850 nm. The small decrease is attributed to the loss of the superlattice contribution to the photocurrent; the large increase in photocurrent below 850 nm is attributed to increased light absorption in the inner buffer layers caused by loss of the superlattice and the outer buffer layers. All these effects are consistent with the band diagram of Figure 10a.

The etching experiments with the large barrier SLS electrodes (Figure 2) indicate that in these particular samples the contribution of the superlattice region to the cathodic and anodic photocurrents is small. Under anodic bias only a very small decrease in photocurrent is seen between 750 and 825 nm after etching; under cathodic bias the photocurrent increases over the whole spectrum after etching. These results indicate that the poor morphology in the more highly strained SLS electrodes causes very low quantum yields for photocurrent generation in the superlattice layers, presumably through high electron-hole recombination rates.

The results of etching experiments with the large-barrier SLS electrode containing a p-doped GaAs epilayer (Figure 4) are consistent with the band diagram of Figure 10b. In this sample, a significant cathodic response is present due to light absorption in the superlattice layers, which disappears when the superlattice layers are removed by etching. Thus, the results in Figures 2 and 4 indicate there is great variability in the photocurrent response of the superlattice layers in 2-eV barrier SLS electrodes, with corresponding variability in the relative contribution of the buffer layers.

The PR spectra in Figures 5 and 6 provide important information that complements the photocurrent data from the small and large barrier SLS electrodes with undoped buffer layers (Figures 2 and 3). The PR spectrum for the 1.7-eV barrier SLS electrode (Figure 6) shows seven peaks. Five are associated with the five predicted allowed ($\Delta n = 0$) transitions in the wells of the sample, one peak at 1.476 eV is associated with a nonallowed transition with $\Delta n = -2$, and two are associated with the two buffer layers; one of the latter two transitions at 1.494 eV overlaps a quantum well transition. The agreement with theory is reasonable (see Table II). Hence, the low-barrier SLS samples exhibit well-defined quantization; this is consistent with the relatively good morphology that is visibly apparent in these samples (smooth and shiny surfaces).

However, while the anodic photocurrent spectrum of this sample (Figure 3B) does show some structure, it is not well-resolved and does not reflect the five quantized transitions present in the SL as clearly and convincingly as the PR spectrum of Figure 6. This is due, in part, to the fact that PR spectra are derivative-like (1st, 2nd, or 3rd depending upon the nature of the optical transition),[5] and therefore are much more sensitive than normal absorption or photocurrent spectra to different optical transitions. In addition, since photocurrent arises from a combination of absorption and transport processes, it is possible that in SLS electrodes the transport processes may broaden the quantization effects and reduce the resolution of the photocurrent action spectra.

Compared to the 1.7-eV barrier SLS, the PR spectrum in Figure 5 for the 2.0-eV SLS electrode is poor; it is very noisy and a reasonable fit of the experimental data could not be achieved. The surfaces of these samples appear milky, resulting in a large amount of light scattering. The poor PR spectra could be caused by poorly defined quantization and/or by the high degree of light scattering. The former explanation is believed to dominate because the PR spectrum of the 2.0-eV barrier SLS electrode with a p-doped epilayer, and with better visible morphology, also did not show well-defined peak structure arising from quantization in the wells. This poor PR spectrum was also consistent with the lack of structure in the photocurrent spectrum (Figure 4) for this sample. Thus, it appears that highly strained, high-barrier SLS electrodes do not have well-defined quantum states in the wells.

Our previously reported results[2,3] for high-barrier SLS electrodes showed pronounced structure in the cathodic and anodic photocurrent spectra. In light of the current experiments and more complete understanding of the behavior of SLS electrodes, we must now conclude that these previous results reflected a photoresponse that was probably influenced more by the buffer layers than by the superlattice layers. We cannot make a precise analysis of the relative contributions of these two regions in the previous results because of the great variability that is evident in the photocurrent behavior of high-barrier SLS electrodes.

On the other hand, the photoresponse of LMS electrodes is very well behaved and highly reproducible, and the contribution of the superlattice layers alone can be unequivocally established. The photocurrent spectra in Figure 8, A and B, for the thick-barrier LMS electrode clearly show eight photocathodic peaks. If the photocathodic peak positions in Figure 8B are assumed to correspond to heavy-hole electron transitions, then they can be matched very well with the theoretically calculated heavy-hole electron transitions if the well width is taken to be 265 Å (see Table III). However, the PR spectra of Figure 9 exhibit 17 optical transitions that can be fitted extremely well to all of the allowed transitions in the quantum wells, taking into account both heavy- and light-hole transitions, if the width of the well is taken to be 285 Å. This difference in well thickness (265 vs 285 Å) is not due to experimental variations in layer thicknesses among samples since repeat PR and photocurrent spectra obtained with samples from the very same initial superlattice wafer showed exactly the same result.

We believe that the PR spectra reflect the true transitions energies and, conversely, that the position of the peaks in the photocurrent spectra do not correspond exactly to the heavy-hole electron transitions energies. This conclusion is based on the fact that, whereas the PR spectra reflect just optical transitions, the photocurrent spectra reflect both optical absorption *and* charge transport and thus involve more complex phenomena and less straightforward interpretation. Also, there is no theoretical basis at the present time for assuming that only heavy-hole transitions should appear in the photocurrent spectra of our samples. The theory of line shapes for the photocurrent spectroscopy of superlattice electrodes remains to be developed and to address such questions as the roles of heavy and light holes, excitonic effects, and miniband formation. It is noted that Figure 9 exemplifies both the high quality of the LMS superlattice samples and the sensitivity of the PR technique in observing critical points in the

absorption spectra of superlattices.

The difference in the cathodic quantum yields between LMS electrodes with an undoped epilayer and a p-doped epilayer is due to photocurrent generated in the p–n junction that exists in the former configuration. The photocurrent from the configuration with the p-doped epilayer is derived only from the superlattice layers; a p–n junction does not exist here. The progressive loss of the peak structure in LMS electrode samples that have been progressively etched is, of course, additional proof that the pronounced cathodic photocurrent peaks arise only from the superlattice layers.

The higher quantum yields for the thin-barrier LMS compared to the thick-barrier LMS electrode result from enhanced tunnelling and miniband formation in the thin-barrier superlattice. The equilvalence of the photocurrent spectra for both SLS and LMS electrodes with either liquid or solid contacts shows that the behavior of superlattice electrodes described here is not related to the nature of the junction material.

Finally, in our previous publications on LMS and SLS electrodes,[1-3] we suggested that changes in the photocurrent action spectra with changes in the redox potential of electron acceptors in solution should serve as evidence for hot electron injection from the superlattice electrodes into solution. However, a detailed quantitative analysis of the kinetics of electron transfer from superlattice electrodes[7] together with the present results on SLS photoelectrodes indicates that this interpretation is not sufficiently general and may not be valid for our previous experimental conditions. Therefore, further experimental work is required to unequivocally establish the importance of hot electron transfer processes in superlattice electrodes.

Acknowledgment. This work was supported by the U.S. Department of Energy, Office of Basic Energy Sciences, Division of Chemical Sciences. The authors are indebted to J. M. Olson of SERI for providing the SLS electrodes and to H. Morkoc and R. Houdrê of the University of Illinois for providing the LMS electrodes. We also thank D. Meissner for useful discussion, and C. Parsons for initial help in setting up the PR experiments.

(7) Nozik, A. J.; Turner, J. A.; Peterson, M. W. *J. Phys. Chem.* **1988**, *92*, 2493.

Direct Observation of Intermediate Ligation States of Hemoglobin

Gérard Simonneaux,* Arnaud Bondon, Christian Brunel, and Patrick Sodano

Contribution from the Laboratoire de Chimie des Organométalliques, UA CNRS 415, Université de Rennes I, 35042 Rennes Cedex, France. *Received November 2, 1987*

Abstract: The ^{31}P NMR spectrum of partially liganded $HbPMe_3$ (HbAo hemoglobin) contains resonances at the normal chemical shift positions of the fully liganded species (R state), in addition to two resonances at intermediate positions. Analysis of the relative magnitude of these four peaks in the absence and in the presence of inositol hexaphosphate shows that PMe_3 binds preferentially to α chains and permits identification of the intermediate species. Plots of the fractional saturation of Hb versus the concentration of unbound PMe_3 exhibit markedly cooperative behavior as evidenced by the sigmoid nature of the binding curve and a large hill coefficient ($n = 2.3$). ^1H NMR studies of the high-field spectra of PMe_3 protons in $HbPMe_3$ are consistent with ^{31}P NMR results.

From the very beginning, the nature and role of intermediates in cooperative ligand binding to hemoglobin (Hb) has been difficult to define.[1] First there is the problem of direct observation of partially liganded states in unmodified hemoglobins. Low-temperature redox trapping of partially liganded HbCO has recently established their existence quantitatively and determined whether the site(s) of CO binding is in the α or β chains.[2] The more difficult problem of obtaining structural information about the intermediates and relating this to the mechanism of cooperativity has typically been approached with modified or hybrid hemoglobins.[3] These studies tend to be contradictory with respect to preferential ligand binding to the α or β chains,[4] but nevertheless, there is a growing evidence for preferred intermediate states. Many of these must have distinct tertiary structure and some[3d,5] may have quaternary structures that are distinct from the T or R state. In this paper, we show that ^{31}P NMR spectroscopy can be used as a direct probe of ligand binding to unmodified Hb. Two distinct intermediates are seen. Both appear to involve preferential binding to the α chains in the T state or in a modified quaternary structure T′.

Results and Discussion

The ligand used is a phosphine, PMe_3, which is small enough to complex Hb. We have previously shown that the iron-bound $^{31}PMe_3$ chemical shifts are sensitive to the presence of the globin: separated NMR signals can be observed for PMe_3 bound to the hemes of the α and β chains in the R state.[6] The ^{31}P NMR spectrum of partially liganded hemoglobin solutions is shown in

(1) (a) Monod, J.; Wyman, J.; Changeux, J. P. *J. Mol. Biol.* **1965**, *12*, 88–118. (b) Koshland, D. E.; Nemethy, G.; Filmer, D. *Biochemistry* **1966**, *5*, 365–385. (c) Perutz, M. F. *Nature (London)* **1970**, *228*, 726–739.

(2) Perrella, M.; Sabbioneda, L.; Samaja, M.; Rossi-Bernardi, L. *J. Biol. Chem.* **1986**, *261*, 8391–8396. Samaja, M.; Rovida, E.; Niggelen, M.; Perrella, M.; Rossi-Bernardi, L. *J. Biol. Chem.* **1987**, *262*, 4528–4533.

(3) (a) Huestis, W. H.; Raftery, M. A. *Biochemistry* **1975**, *14*, 1886–1892. (b) Knowles, F. C. *Arch. Biochem. Biophys.* **1984**, *230*, 327–334. (c) Fung, L. W. M.; Minton, A. P.; Ho, C. *Proc. Natl. Acad. Sci. U.S.A.* **1976**, *73*, 1581–1586. (d) Miura, S.; Ho, C. *Biochemistry* **1982**, *21*, 6280–6287.

(4) Reisberg, P.; Olson, J. S.; Palmer, G. *J. Biol. Chem.* **1976**, *251*, 4379–4383. For a recent review see: Nasuda-Kouyama, A.; Tachibana, H.; Wada, A. *J. Mol. Biol.* **1983**, *164*, 451–476.

(5) (a) Viggiano, G.; Ho, C. *Proc. Natl. Acad. Sci. U.S.A.* **1979**, *76*, 3673–3677. (b) Miura, S.; Ho, C. *Biochemistry* **1984**, *23*, 2492–2499. (c) Brozozowski, A.; Derewenda, Z.; Dodson, E.; Grabowski, M.; Liddington, R.; Skarzynski, T.; Vallely, D. *Nature (London)* **1984**, *307*, 74–76. (d) Smith, F. R.; Ackers, G. K. *Proc. Natl. Acad. Sci. U.S.A.* **1985**, *82*, 5347–5351. Inubushi, T.; D'Ambrosio, C.; Ikeda-Saito, M.; Yonetani, T. *J. Am. Chem. Soc.* **1986**, *108*, 3799–3803.

0002-7863/88/1510-7637$01.50/0